# Performance analysis of an Aero Engine with Interstage Turbine Burner

Yin, Feijia; Gangoli Rao, Arvind

**DOI**
10.1017/aer.2017.93

**Publication date**
2017

**Document Version**
Accepted author manuscript

**Published in**
The Aeronautical Journal

**Citation (APA)**
Yin, F., & Gangoli Rao, A. (2017). Performance analysis of an Aero Engine with Interstage Turbine Burner. *The Aeronautical Journal*, *121*, 1605-1626. https://doi.org/10.1017/aer.2017.93

# Performance Analysis of an Aero Engine with Interstage Turbine Burner

Feijia Yin[1] Arvind G. Rao[2]

*Faculty of Aerospace Engineering, Delft University of Technology*
*Delft, the Netherlands, 2629 HS*

**The historical trends of reduction in fuel consumption and emissions from aero engines have been mainly due to the improvement in the thermal efficiency, propulsive efficiency and combustion technology. The engine Overall Pressure Ratio (OPR) and Turbine Inlet Temperature (TIT) are being increased in the pursuit of increasing the engine thermal efficiency. However, this has an adverse effect on engine NOx emission. The current paper investigates a possible solution to overcome this problem for future generation Very High Bypass Ratio (VHBR)/Ultra-High Bypass Ratio (UHBR) aero-engines in the form of an Inter-stage Turbine Burner (ITB). The ITB concept is investigated on a next generation baseline VHBR aero engine to evaluate its effect on the engine performance and emission characteristics for different ITB energy fractions. It is found that the ITB can reduce the bleed air required for cooling the HPT substantially (around 80%) and also reduce the NOx emission significantly (> 30%) without penalizing the engine specific fuel consumption.**

**[1] PhD Researcher, Faculty of Aerospace Engineering, Kluyverweg 1, 2629HS, Delft**
**[2] Associate Professor, corresponding author, Faculty of Aerospace Engineering, A.gangolirao@tudelft.nl, Kluyverweg 1, 2629HS, Delft**

## Nomenclature

*Abbreviation*

| | | | |
|---|---|---|---|
| BPR | = | Bypass Ratio | |
| EINOx | = | NOx Emission Index | [g/kg] |
| GITB | = | Geared Interstage Turbine Burner | |
| HPC | = | High Pressure Compressor | |
| HPT | = | High Pressure Turbine | |
| ISA | = | International Standard Atmosphere | |
| ITB | = | Interstage Turbine Burner | |
| LPC | = | Low Pressure Compressor | |
| LPT | = | Low Pressure Turbine | |
| NGV | = | Nozzle Guide Vanes | |
| OPR | = | Overall Pressure Ratio | |
| PSR | = | Perfectly Stirred Reactor | |
| SLS | = | Sea Level Static | |
| ST | = | Specific Thrust | [N.s/kg] |
| TSFC | = | Thrust Specific Fuel Consumption | [g/kN/s] |
| VHBR | = | Very High Bypass Ratio | |
| UHBR | = | Ultra High Bypass Ratio | |

*Symbol*

| | | | |
|---|---|---|---|
| $\dot{m}$ | = | mass flow rate | [kg/s] |
| $\eta$ | = | efficiency | |
| $\pi$ | = | pressure ratio | |
| $\Delta$ | = | Variation with respect to baseline | |

## I. Background and Motivation

Propulsion technologies have been at the forefront of aeronautics. The large reduction in the fuel consumption of a modern aircraft when compared to the early jet-powered aircraft, is mainly due to the reduction in fuel consumption of engines [1]. Even though the efficiency of aircraft and engine have increased substantially over the years (approx. 1.3% every year in terms of fuel burn per passenger km), it has been outpaced by the growth in aviation (approx. 4.8% per year). It has now been established that emissions from civil aviation can no longer be neglected because of the increase in air traffic and due to the fact that the aircraft emission occurs within the sensitive layers of the atmosphere, near the tropopause [2, 3]. With global warming becoming one of the main challenges faced by humanity, there is an increased impetus to reduce emissions from aero engines. The Advisory Council for Aviation Research and Innovation in Europe (ACARE) has set ambitious goals for 2050 to reduce $CO_2$ emission by 75%, NOx emissions by 90%, and the perceived noise by 65% with respect to a baseline aircraft in service in the year 2000 [4].

The $CO_2$ emission is directly associated with the consumption of fossil fuels. Therefore, reducing the fuel consumption helps to reduce $CO_2$. Historically, the reduction in fuel consumption has been realized by an increase in the thermal efficiency (increasing OPR, TIT, and component efficiencies) and the propulsive efficiency (by lower FPR and higher BPR). The OPR has more than doubled in the past four decades, as summarized in Figure 1. The latest turbofans have reached an OPR of more than 50. Following this development trend, it is very likely that the next generation of VHBR / UHBR engines would reach an OPR close to 70.

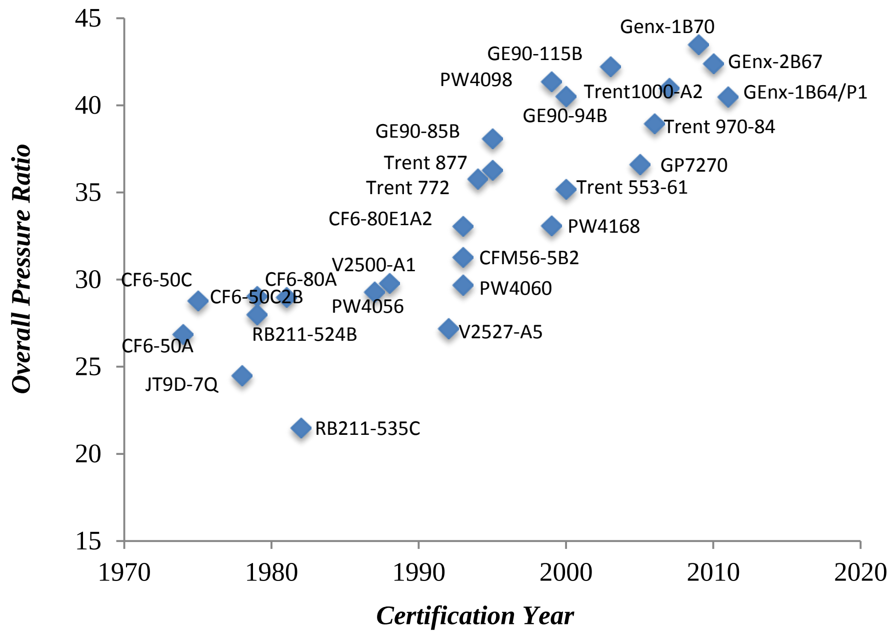


**Figure 1: Engine overall pressure ratio increment. (Data Source: the engine certification data sheet of ICAO)**

As a result of high OPR, the TIT has to be increased as well to realize an optimum Brayton cycle [5]. Figure 2 shows the historical trend in TIT and the development of maximum allowable metal operating temperature. The average increase in TIT has been around 19°K/year, which is substantially higher than the increase in operating metal temperature of around 5°K/year. This discrepancy is compensated by the sophisticated cooling techniques. When the TIT exceeds allowable metal operating temperature significantly, a large amount of bleed air is required to cool the turbine stage. The bleed air used for turbine cooling bypasses the combustor and does not completely participate in the main cycle, thereby imposing penalties on the cycle performance. Horlock, et.al [6] and Wilcock, et.al [7] have modeled the gas turbine performance incorporating the effect of bleed air and have demonstrated the performance penalties due to turbine cooling and higher compressor work required for pressurizing the bleed air.

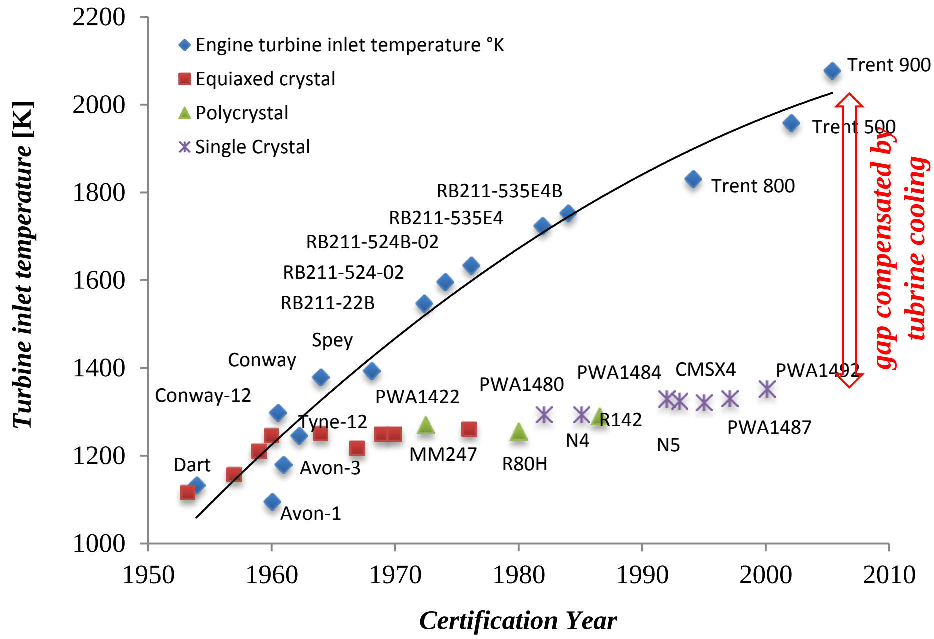


**Figure 2: Evolution of turbine inlet temperature and metal operating temperature over the years (Figure reproduced by data from Rolls Royce jet engine).**

Moreover, increasing OPR and TIT increases NOx emissions for a given combustor technology [8]. In Figure 3, the historical trend in Landing Takeoff cycle (LTO) NOx emissions based on ICAO engine certification databank is illustrated [9]. For a given period when the combustion technology remained unchanged, the NOx emission increased with increase in OPR. The reduction in NOx emission due to the advancement in the combustion technology can be seen in the figure. It is also evident from the figure that even with advanced combustion technology, it is difficult to satisfy the ACARE objectives (depicted by the solid line at the bottom of the figure). Therefore, breakthrough technologies in engine architecture and combustion technology should be explored.

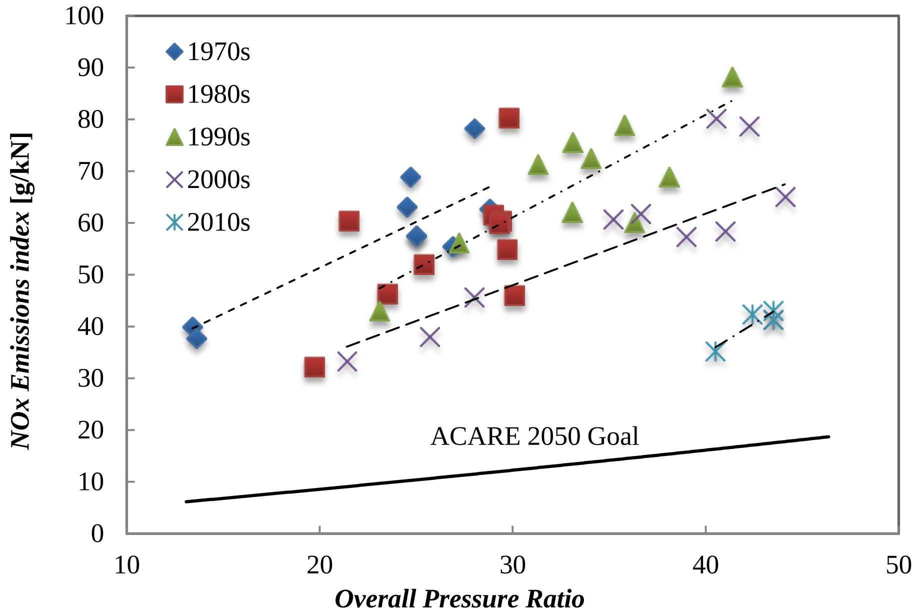


**Figure 3: The LTO NOx emissions index versus OPR at SLS. (Figure produced using the engine type certification data sheet of ICAO)**

The geared turbofan engine (GTF) [10] has been a significant step in aircraft engine architecture and offers significant advantages in terms of increasing the engine propulsive efficiency without deteriorating the thermal efficiency. In the coming years, the GTF architecture would be scaled up for the wide-body aircraft. Even though, the conflicts between reduction in $CO_2$ emission (due to the increase in OPR and TIT) and the increase in the NOx emission cannot be eliminated. The current turbofan engine architectures (conventional as well as the GTF) do not provide any significant advantages in terms of reducing the impact of high OPR and TIT on the NOx emission. This criterion would play an important role in determining the course of evolution in future aero engine architecture. This paper provides an improvement in the GTF engine architecture such that $CO_2$ emission reduction due to high OPR and TIT can be obtained without increasing the NOx emission.

The intercooled engine is another concept that is being actively investigated by researchers [11-13] as an option to further increase engine OPR. Using intercooling reduces the air temperature at the inlet of HPC, thereby reducing the combustor inlet temperature for given OPR. The reduction in combustor inlet temperature is beneficial in reducing the NOx emissions. On the other hand, a lower combustor inlet temperature increases the fuel required to achieve a given TIT, which is not favorable for the thermal efficiency of the cycle unless the TIT is reduced. For lower TIT, the cycle specific thrust is reduced, increasing the overall size and installation penalty of the engine. Not to mention that incorporating a heat exchanger in the core is extremely challenging and will result in a substantially increase in the overall engine weight. The heat exchanger will also result in pressure losses, both on the core side as well as the bypass side.

## II. Problem identification

The main problem of increasing OPR and TIT in a turbofan can be summarized as:

- Increased complexity and use of superalloys in the High Pressure Compressor (HPC)
- Increased weight of the engine due to the increased number of the HPC stages and the use of superalloys for compressor blades
- The increase in TIT would increase the requirement of cooling air to limit the blade material temperature within its operating range
- The increase in OPR would increase the temperature of the bleed air used for turbine cooling, thereby increasing the bleed mass flow required for cooling the turbine blades even further
- High OPR and TIT result in increased NOx emission
- The increase in TIT results in an increases in gas dissociation effect and the associated loss in the cycle thermal efficiency.

Despite all the challenges, it is still worthwhile to increase the OPR and TIT because of the fuel burn reduction that can be obtained. An engine architecture, which would be able to negate some of the disadvantages mentioned above, would be desirable. The advanced GTF engine with an Inter-stage Turbine Turner (ITB), described in this paper, is one such architecture.

The ITB is an additional combustor located in between the HPT and LPT, replacing the inter-turbine duct in a gas turbine engine. This dual combustor configuration provides different possibilities to design an ITB engine, amongst which, two are illustrated in Figure 4. In Figure 4 a), the inlet temperatures of HPT and LPT are kept identical at the maximum allowable temperature (indicated by the upper dashed line). As a result, the specific power output increases significantly, but at the expense of increased fuel consumption. This architecture is interesting for military engines where the specific thrust is a key parameter driving the engine design. If one attempts to design a civil aero-engine using such architecture, the temperature increase through ITB should be reduced, as demonstrated by the lower dashed line in Figure 4 a). This way a compromised configuration, having higher specific thrust and less penalty in the fuel consumption, is realized. Alternatively, if the specific thrust should be kept constant, then adding an ITB helps to reduce the HPT inlet temperature, as illustrated in Figure 4 b). Accordingly, the HPT cooling requirement and associated loss are reduced. Moreover, the NOx emission decreases due to lower heat addition and lower TIT.

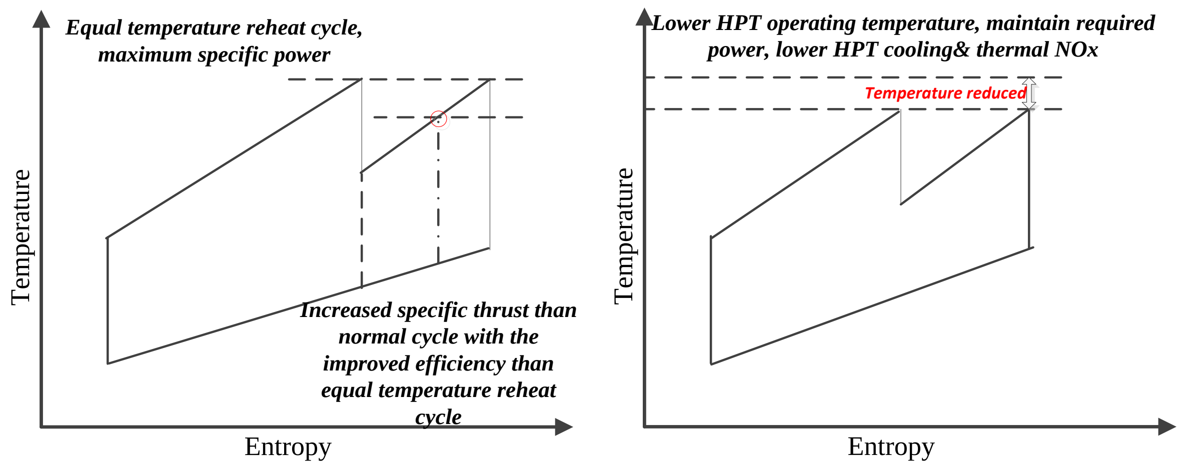


*a) Higher specific power output cycle* *b) Lower turbine cooling and NOx cycle*

**Figure 4: T-S diagram of a reheat cycle for different purposes.**

Research on ITB in aero engines is not new. In Ref. [14-19], the application of ITB in turbojet or the low Bypass Ratio (BPR) turbofan engines for military aircraft has been studied. Conventionally, a fighter aircraft utilizes an afterburner to improve the specific thrust. However, the thermal efficiency of the afterburner is low because heat is being added in the afterburner at low pressure in the thermodynamic cycle, which is detrimental to the thermal efficiency. An ITB engine is thermodynamically more efficient than an engine with an afterburner because the location of ITB is before LPT, where the operating pressure is relatively high. In the reference [14, 15], the ITB has been applied in a conventional turbojet and low bypass turbofan respectively. The results show that ITB engine has lower TSFC than an engine equipped with afterburner, while maintaining a higher specific thrust than a normal engine without afterburner. In [20], a mission analysis has been performed on a turbofan engine with ITB applied for a long range mission. This study shows a slight benefit in mission fuel burn by the ITB engine over a conventional engine with a 180 K lower turbine inlet temperature realized in the ITB engine. This reduction in TIT implies a potential reduction in NOx emission.

Since the ITB is followed by LPT, the LPT inlet temperature is increased due to the presence of ITB, which depending on the temperature can increase the LPT cooling requirement and may penalize the thermal efficiency. Therefore, it is essential to investigate the cooling requirement of both HPT and LPT in an ITB engine. Liew et. al.

[21] have included correlation curves for turbine cooling prediction given by Walsh and Fletcher in [22]. In their analysis, the ITB exit temperature was below the maximum allowable metal temperature to avoid the LPT cooling.

The aim of this paper is to quantify the effects of an ITB on the NOx emission and on the cooling requirements of HPT and LPT, and to evaluate the performance of a next generation geared VHBR turbofan engine with ITB. A sophisticated in-house turbine cooling model has been integrated .

## III. Engine configurations

Following civil aero engine development trend, a VHBR turbofan engine with a geared system representing the state-of-art technology in the year 2025-2030 is used as a baseline engine in the current study. Accordingly, a contemporary ITB engine configuration (named as advanced GITB turbofan engine) is derived. The conceptual comparison of these two engine layouts is presented in Figure 5. The upper part of the figure is the GITB turbofan engine, whereas the bottom part is the advanced GTF baseline engine. The installation effects of introducing ITB in an engine is not dealt with in the current paper, however it can be expected that the engine length increases due the incorporation of ITB. The work in [20] shows that incorporating ITB could reduce the fan diameter. Thus, the installation effects of ITB should not be significantly different than a similar turbofan engine. Moreover, it can be observed that the shape of the ITB differs from that of the main combustor to enable the flow recirculation and to increase the residence time.

The station number is defined in Table 1, and is valid in the whole paper if not mentioned otherwise. The LPT inlet or ITB exit is defined as station 46. Since the ITB is positioned downstream of the HPT where the flow velocity is higher, the energy input into the ITB has been kept intentionally lower than that of the main burner to minimize the pressure loss through the ITB and to reduce the losses in thermal efficiency.

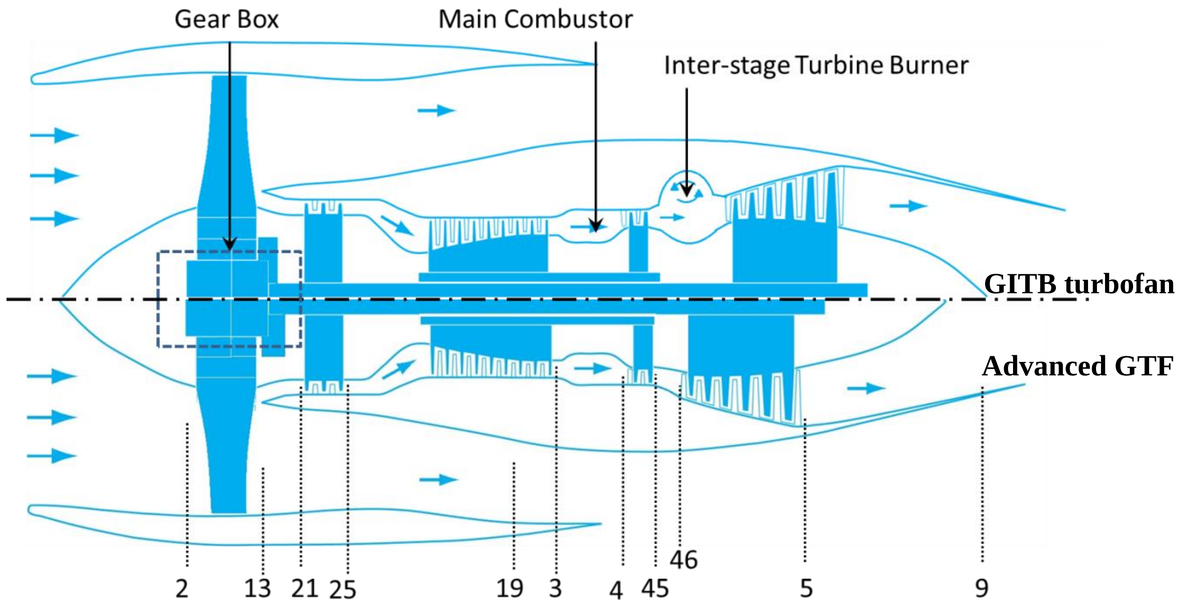


**Figure 5: Engine configuration comparison.**

**Table 1: Engine station number definition**

| ***Station number*** | ***Description*** |
|---|---|
| 2 | Fan inlet |
| 21 | Fan core exit |
| 25 | LPC exit |
| 3 | HPC exit |
| 4 | Combustor exit |
| 45 | HPT exit |
| 46 | LPT inlet/ITB exit |
| 5 | LPT exit |
| 9 | Core nozzle exit |
| 13 | Fan bypass exit |
| 19 | Bypass nozzle exit |

The baseline component efficiencies for both types of engines are defined in Table 2. Since the amount of fuel injected into ITB is lower than the main combustor, the pressure loss in ITB is expected to be lower. The turbine efficiency mentioned in Table 2 is the uncooled efficiency. The loss due to cooling has been taken into account as explained in the later part of this paper.

**Table 2: Baseline component performance parameters**

| *Component* | *Performance parameter* | *Notation* | *Datum value* | *Unit* |
|---|---|---|---|---|
| Fan | polytropic efficiency | $\eta_{fan}$ | 93 | % |
| LPC | polytropic efficiency | $\eta_{LPC}$ | 93 | % |
| HPC | polytropic efficiency | $\eta_{HPC}$ | 91 | % |
| Main combustor | Combustion efficiency | $\eta_{CC}$ | 99.9 | % |
| | pressure ratio | $\pi_{CC}$ | 0.95 | [-] |
| HPT | Uncooled polytropic efficiency | $\eta_{HPT}$ | 93 | % |
| ITB | Combustion efficiency | $\eta_{ITB}$ | 99.7 | % |
| | pressure ratio | $\pi_{ITB}$ | 0.97 | [-] |
| LPT | Uncooled polytropic efficiency | $\eta_{LPT}$ | 92.5 | % |
| HP shaft | Mechanic efficiency | $\eta_{mHPT}$ | 99.5 | % |
| LP shaft | Mechanic efficiency | $\eta_{mLPT}$ | 99.3 | % |
| Bypass duct | Relative pressure loss | $\Delta p_t / p_{tin}$ | 2 | % |

## IV. Modelling Approach

The complete model framework used in the current analysis comprises of two modules: an engine performance module with a detailed turbine cooling module, and an in-house emission prediction module.

### A. The engine performance module

To estimate the engine performance, a zero-D thermodynamic model is created using the Gas Turbine Simulation Program (GSP) [23]. In accordance with the engine configuration, the layout of this engine model for the GITB turbofan engine is depicted in Figure 6. The main gas path of the engine consists of inlet, fan, LPC, HPC, main combustor, HPT, ITB, LPT, core convergent nozzle, bypass duct, and bypass convergent nozzle. The bleed control components numbered from 2-6 and 9 are applied to specify the turbine cooling air requirement either in the form of the absolute air mass flow rate or a fraction of the inlet mass flow rate to the HPC ($\dot{m}_c/\dot{m}_{25}$). In the current research, the latter one is used. The model has a thrust controller, ( shown by component 8), which maintains the thrust of the engine to the specified value. The performance calculation procedure is the same as presented in [5]. Moreover, as far as the second combustion chamber is concerned, the gas composition at the inlet of ITB is significantly different than that of a conventional burner since part of the oxygen has been consumed by the first combustor. The gas model in GSP is used to calculate the composition of the vitiated air. The engine off-design performance is derived from the design condition with the generic component maps included. To predict the turbine cooling air requiremet, an in-house turbine-cooling model has been employed. A detailed information regarding this cooling model will be given in the following subsections.

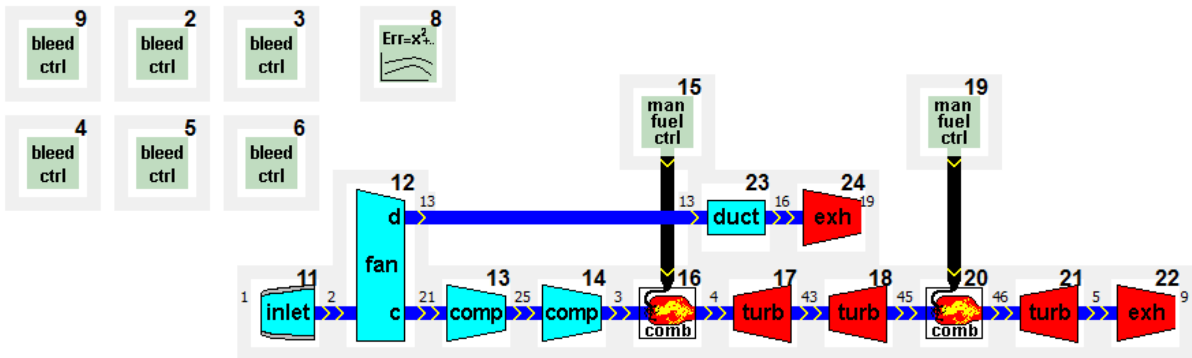


**Figure 6: Layout of a turbofan with ITB.**

## B. The turbine cooling module

In the preliminary engine design phase, it is a common practice to apply empirical correlations to predict turbine cooling air mass flow rate [22]. Most of the correlations behave linearly and provide reasonable prediction within a narrow temperature range. But as the engine OPR and TIT increase, the cooling requirements behave in a non-linear manner and cannot be predicted correctly by these linear models, resulting in significant performance deviation. Therefore, it is essential to have an accurate turbine cooling model, which is capable of capturing the nonlinear characteristics of cooling air fraction, in predicting the amount of cooling air required for maintaining the metal temperature within the operating regime.

An in-house turbine cooling module is built which takes into account both internal and external cooling techniques used in an actual turbine vane and blade. The overall turbine cooling model scheme is shown in Figure 7. The internal cooling scheme consists of rib turbulated channel cooling, jet impingement cooling and pin fin cooling while the external heat transfer consists of film cooling. The arrangement of these cooling modules follows a typical profile used in modern air-cooled turbine blade as presented in Figure 8.

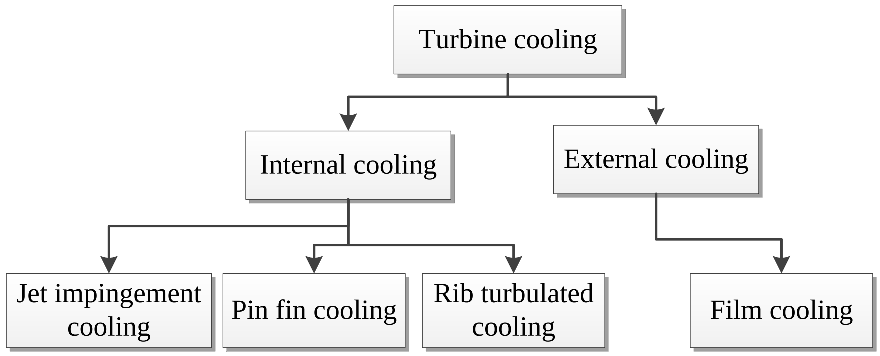


**Figure 7: Turbine cooling scheme.**

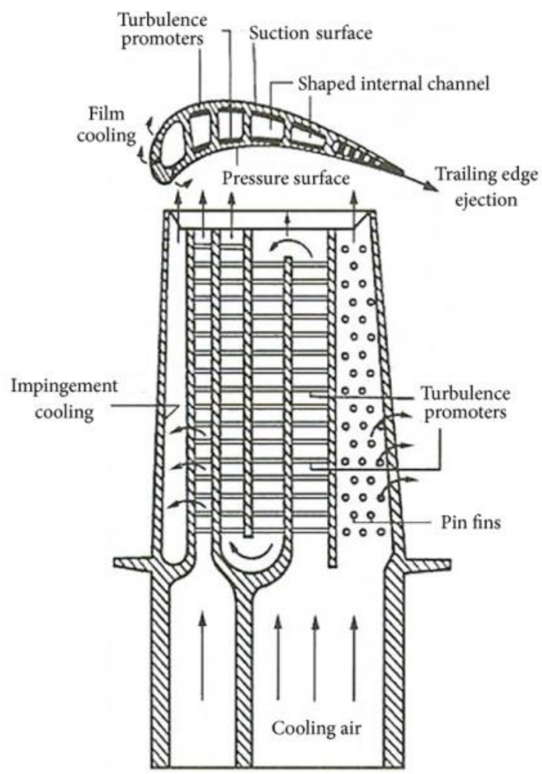


**Figure 8: Design concept of a modern cooled gas turbine blade [24].**

The cooling module calculates the mass flow rate of cooling air required for a single turbine vane or blade. By multiplying it by the total number of blades and vanes, the total mass flow rate of cooling air required for a turbine stage can be evaluated. The cooling air mass flow rate is dictated by several parameters, including the maximum allowable metal operating temperature, the bleed air pressure, the bleed air temperature, the turbine operating temperature and pressure. The iterations are executed till the heat flux between the cooling air and the hot gas reaches an equilibrium condition. This cooling model has been validated with the NASA Energy Efficient Engine

(E3) engine cooling system as described in [25, 26]. Detailed information with respect to the turbine geometry and the turbine cooling model can be found in [27]. In the current research, the maximum allowable metal operating temperature is assumed as 1450 K, which matches with materials available in 2025.

The cooling arrangement in the GITB turbofan engine can be seen in Figure 9. The cooling flow for the first stage HPT and the second stage HPT is considered separately. For the LPT cooling, it is assumed that only the first stage of LPT requires cooling (as the temperature of the gas drops below the metal operating temperature in the later stages), therefore, the LPT is not split into various stages. The cooling air is bled from different stages of the HPC depending on the operating pressure of the turbine stage. The same cooling arrangement is considered for the advanced GTF engine.

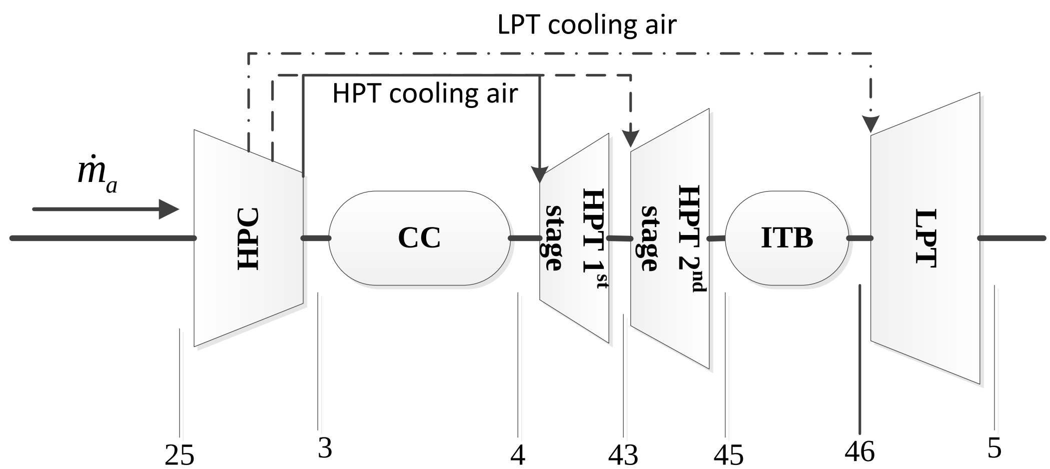


**Figure 9: Layout of the cooling airflow in the GITB turbofan engine.**

Turbine cooling has a significant effect on the turbine efficiency. Research has been conducted to investigate the effect of cooling on the overall efficiency of a turbine stage. Hartsel [28] has demonstrated two analytical models to estimate the efficiency of a cooled turbine (Harsel eff.). Kurzke [29] redefined the turbine efficiency (mainstream pressure mixed eff.) considering different bookkeeping approaches for single stage and multi-stage turbines. As for the loss due to mixing and the aerodynamic loss, the prediction is not straightforward. First, the cooling flow coming out of a turbine blade tends to affect the aerodynamic profile, which influences the turbine efficiency; moreover, when the two flow streams at different temperatures mix, the total entropy increases, resulting in additional losses. Young and Horlock [30] have attempted to provide distinguished definitions from this perspective (fully reversible mixed eff.).

By considering various methodologies discussed in the literature and considering the expected technology improvement in future, a compromised effect of turbine cooling based on the following assumptions has been considered in this paper (indicated by *New Estimated Eff.*).

- The cooling flow of the NGV at any turbine stage completely mixes with the mainstream before the expansion through the blade.
- 50% of the cooling air for the first stage HPT rotor participates in the work output of the turbine.
- The second stage HPT rotor cooling air mixes with the mainstream after the expansion, therefore, does not contribute to the turbine power output.

As a result of above considerations, an estimation has been made in this paper. Accordingly, every unit percentage of the turbine cooling increase will cause roughly 0.6% reduction in the turbine polytropic efficiency (as indicated by "*new estimated eff.*" in Figure 10). This will be applied in the current paper to calculate the cooled turbine efficiency.

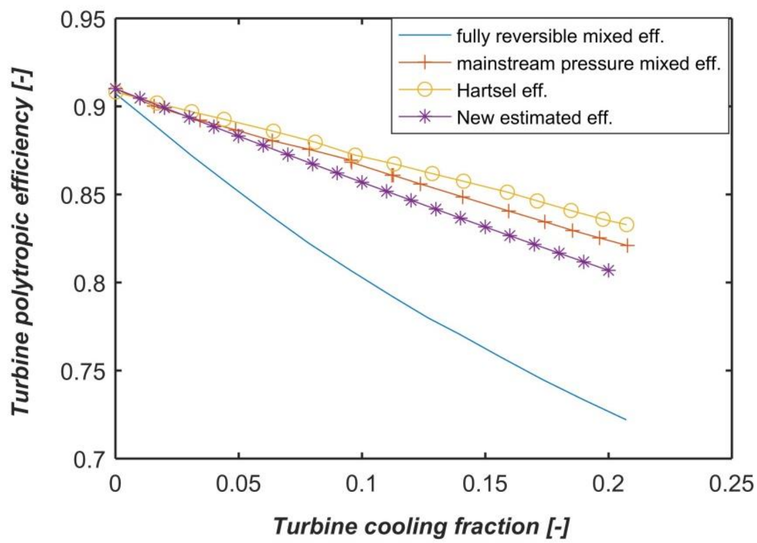


**Figure 10: Various methodologies to account for the effect of turbine cooling (figure reproduced using data provided in [31]).**

### C. The NOx emission prediction module

It is known that the thermal NO dominates the NOx emission in aero-engines. As the name suggests, the thermal NO production increases exponentially when the temperature within the combustor exceeds 1800K. Several parameters, including, local equivalence ratio, residence time, temperature, concentration of species, and type of fuel used, are responsible for the total NOx emission. The complex chemical mechanisms make the prediction of NOx emission challenging. From the engine performance point of view, it is a common practice to use some empirical or semi-empirical equations provided in the literature. For example, in [32] a semi-empirical equation has been provided, where the NOx emission depend on the combustion chamber volume, the stoichiometric flame temperature, the primary zone temperature, and the combustor inlet pressure. There are also more NOx emission prediction models presented in [8, 33]. Although these emission prediction tool consider various parameters, they are mainly valid for engines using conventional combustion chamber, and therefore not suitable for new types of the combustion system, for instance, the sequential combustion chambers.

The ITB engine architecture and properties are substantially different than that of a conventional turbofan engine using conventional combustor. First, the oxidant of the ITB is vitiated air where part of the $O_2$ has been consumed in the first combustor and the products of combustion from the first combustor form a significant part of the incoming gases. Secondly, the inlet temperature and the flow velocity of the ITB is different from that of the conventional combustor because of the increased temperature and the lower pressure. Moreover, the NOx produced by the main combustor, which is present in the gases, might dissociate in the ITB [34]. Therefore, it would be inappropriate to use the existing empirical methods for emission prediction of the GITB engine.

To facilitate the NOx prediction for the GITB engine, an in-house emission prediction tool has been developed using Cantera's reactor networks [35]. The basic geometry of the combustor is created based on the methodology described by Shakariyants [36]. A complete reactor network is constructed using Perfectly Stirred Reactors (PSR), which are integrated to represent different combustion zones within a combustion chamber. The network is displayed in Figure 11. The entire combustor is divided into three combustion zones, including primary zone (divided into two subsections), secondary zone, and dilution zone (divided into two sections). Also, a mixing zone is included. The combustor volume is calculated beforehand based on the operating conditions. By specifying the air fractions distributed in the different combustion zones, the residence time and the equivalence ratio of each combustion zone is determined.

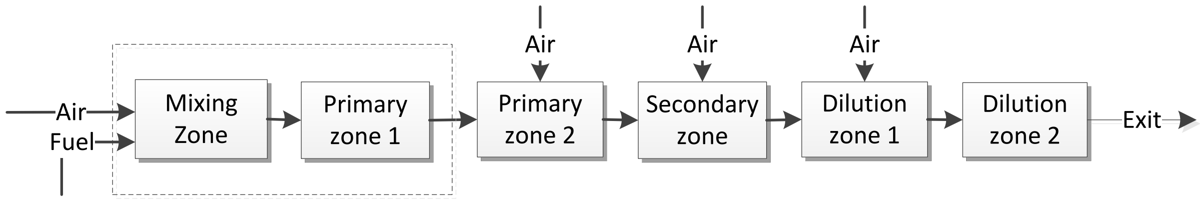


**Figure 11: Chemical reactor network for the first and the second combustion chambers in the current paper analysis.**

To predict the emissions, a detailed chemical reaction mechanism is required. Kerosene is a complex fuel, which contains petroleum byproducts in which the dominant mass fractions are of higher hydrocarbon. Chromatograph of kerosene shows the presence of components ranging from butane to tricosane. The average chemical formula varies from $C_{10.9}H_{22}$ to $C_{12}H_{23}$. There is a variance of composition in kerosene from one source to another, and this has led to several surrogate compounds being proposed for kerosene by different researchers. Surrogates can be a mix representing the overall physical property of kerosene or chemical surrogate representing the chemical property. The mixture describing both these properties is called as comprehensive surrogates. Alkane part of surrogate fuels is well represented by n-Decane and few other compounds; however, the major problem lies with oxidation of aromatic cyclic hydrocarbons. The kerosene reaction is a complex one involving hundreds of species and reactions [37]. The complicated set of reactions occurring between free hydrogen atoms and aromatic hydrocarbons lead to the formation of soot, which is a very important emission species to be predicted. In general, the prediction of emissions like NOx and CO is strongly dependent on the temperature and flow field, which is strongly dependent on the kinetics of reacting species. For the current study, the Aachen Surrogate containing 77.7% n-Decane and 22.3% n-Propyl Benzene is used. This mechanism has been developed and tested at TU Aachen by Honnet et al. [38] and consists of 119 species and 527 reactions.

The validation of this combustion reactor network has been performed with respect to an existing CF6 engine [39]. After the validation, the same methodology is used to design a combustion chamber and estimate the emissions from the baseline VHBR GTF engine and the proposed GITB engine. Even though the combustor used in this analysis is different than a probable future combustion system, which might find its place in the next generation of engines like the Lean Direct Injection (LDI) combustor [40, 41], the main aim of the current research is to evaluate the effect of the two engine architectures on the overall emissions. Therefore, the relative change in emissions is more important than the absolute emission

## V. Results and discussions

The cycle optimization is performed at cruise condition, whereas, the turbine cooling requirement is estimated at the SLS ISA+15K condition and applied to cruise condition. The MATLAB fmincon optimizer using Sequential Quadratic Programming (SQP) algorithm is implemented for the cycle optimization [42]. The objective is to minimize the cruise engine Thrust Specific Fuel Consumption(TSFC). Fundamentals of the SQP algorithm has been thoroughly discussed by Nocedal and Wright in [43].

### A. Engine performance optimization

The thrust requirement at cruise and Sea Level Static (SLS) conditions are provided in Table 3. The cruise condition is defined at an altitude of 11 km and Mach number of 0.85, where the cycle is optimized to minimize the TSFC. The turbine cooling airflow rate and the thermal NOx emission are evaluated at the hot day SLS condition.

**Table 3: Engine thrust requirement**

| | ***Altitude [km]*** | ***Mach number [-]*** | ***Ambient condition*** | ***Thrust [kN]*** |
|---|---|---|---|---|
| Cruise | 11 | 0.85 | ISA | 47 |
| SLS | 0 | 0 | ISA+15 K | 299.8 |

The same design space for the GTF and the GITB engine are defined in Table 4. The OPR is constrained for two reasons. First, it prevents the HPC exit temperature from exceeding the material limit; secondly, increasing the OPR results in smaller blade size of the HPC last stage, where the tip clearance loss become dominant [44]. An ITB energy fraction defined in Eqn.(1), is applied to indicate the amount of fuel added in the ITB. An ITB energy fraction of zero implies that all the energy is added in the main combustor, similar to the baseline GTF engine. The optimization is executed at the ITB energy fraction ranging from 0 to 0.35 with a step change of 0.05. The turbine efficiency varies with respect to the turbine cooling air fraction.

$$ITB\ energy\ fraction = \frac{\dot{m}_{f_2} \times LHV_{f2}}{\dot{m}_{f_1} \times LHV_{f1} + \dot{m}_{f_2} \times LHV_{f2}} \tag{1}$$

where $\dot{m}$ and LHV are the mass flow rate and the Lower Heating Value of given fuel; the subscript $f_1$ and $f_2$ indicate the fuel for the first combustor and the ITB respectively.

**Table 4: The design space and constraints for the cycle optimization.**

| ***Variation range of design parameters*** | | ***Constraints*** | |
|---|---|---|---|
| FPR | [1.2, 1.8] | OPR | <= 70 |
| LPC pressure ratio | [1.4, 5.0] | FN (kN) | = 47 |
| HPC pressure ratio | [8, 20] | $\dot{m}_a$ at the engine inlet | Constant |
| Tt4 (K) | [1300, 1900] | | |
| BPR | [8, 15] | | |
| ITB energy fraction | [0, 0.35] | | |

Among all the optimization cases, the selected examples are presented in Table 5. The $\dot{m}_{c\_HPT}$ is the HPT cooling air mass flow rate, the $\dot{m}_{c\_LPT}$ is the LPT cooling air mass flow rate, and the $\dot{m}_{25}$ is the overall air mass flow rate at the HPC inlet. The BPR of each engine reaches the upper limit to maximize the propulsive efficiency. Since the specific thrust ($\dot{m}_a/FN$) is kept constant, the FPR of each cycle also remains unchanged. Moreover, the LPC pressure ratio in all cases reaches the maximum. This can be explained from two aspects. First, at a lower ITB energy fraction, the HPT inlet temperature increases and thereby increasing the HPT cooling air requirement. The optimizer tends to reduce the HPT work output by splitting the compression work more towards LPC. Secondly, when the ITB energy fraction increases, the optimizer tends to increase the ITB operating pressure by reducing the HPC pressure ratio, which is thermodynamically beneficial.

**Table 5: Engine optimization results at Cruise.**

| ***Design parameters*** | ***ITB energy fraction*** | | | | |
|---|---|---|---|---|---|
| | 0 | 0.1 | 0.2 | 0.3 | 0.35 |
| BPR | 15 | 15 | 15 | 15 | 15 |
| FPR | 1.44 | 1.44 | 1.45 | 1.45 | 1.45 |
| LPCPR | 5 | 5 | 5 | 5 | 5 |
| HPCPR | 9.69 | 9.69 | 9.69 | 9.69 | 9.68 |
| HPT IT [K] | 1900 | 1689 | 1540 | 1431 | 1387 |
| LPT IT [K] | 1177 | 1182 | 1190 | 1202 | 1209 |
| *Output parameters* | | | | | |
| TSFC [g/kN/s] | 13.6 | 13.7 | 13.8 | 14.1 | 14.2 |
| HPT turbine cooling fraction ($\dot{m}_{c\_HPT}/\dot{m}_{25}$) [%] | 38.7 | 27.3 | 17.6 | 10.3 | 7.6 |
| LPT turbine cooling fraction ($\dot{m}_{c\_LPT}/\dot{m}_{25}$) [%] | 0 | 0 | 0.02 | 0.09 | 0.14 |

The variation of HPT and LPT inlet temperature for hot-day static thrust is shown in Figure 12. It shows that the HPT inlet temperature decreases substantially with the increase in the ITB energy fraction. The increase in LPT inlet temperature, on the other hand, is confined by the constraint of constant specific thrust. This helps to reduce the energy wastage in the exhaust heat, thereby improving the thermal efficiency of the reheat cycle.

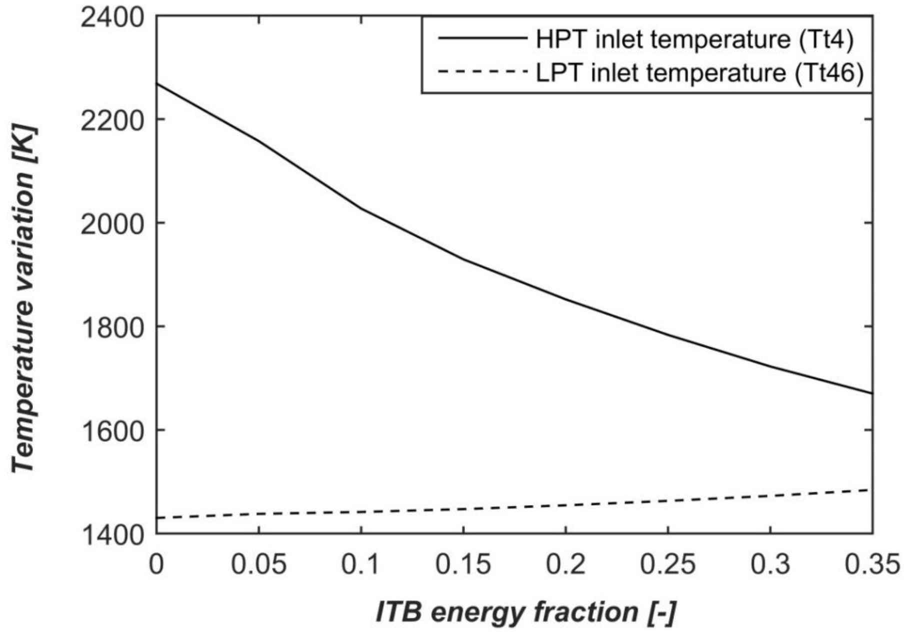


**Figure 12: Variation of turbine inlet temperatures versus ITB energy fraction at SLS.**

### B. Effects of ITB on engine performance and turbine cooling

In Figure 13, Figure 14, and Figure 15, one can see the variation of the HPT cooling, the variation of the LPT cooling and the variation of the cruise TSFC with respect to the ITB energy fraction respectively. One can see that the HPT cooling fraction reduces substantially as ITB energy fraction increases due to the reduction in the HPT inlet temperature. With an ITB energy fraction of 0 (corresponding to the VHBR GTF engine), the highest HPT cooling air fraction is required. This reduction in cooling airflow improves the HPT efficiency substantially as can be observed from Figure 16. It can be observed that LPT cooling is not required for ITB energy fraction below 0.15. It also can be observed from Figure 15 that for ITB energy fraction below 0.15, the increase in TSFC is less than 1%. When the ITB energy fraction increases further, the deterioration in the TSFC increases due to the negative effect of the ITB on cycle thermal efficiency.

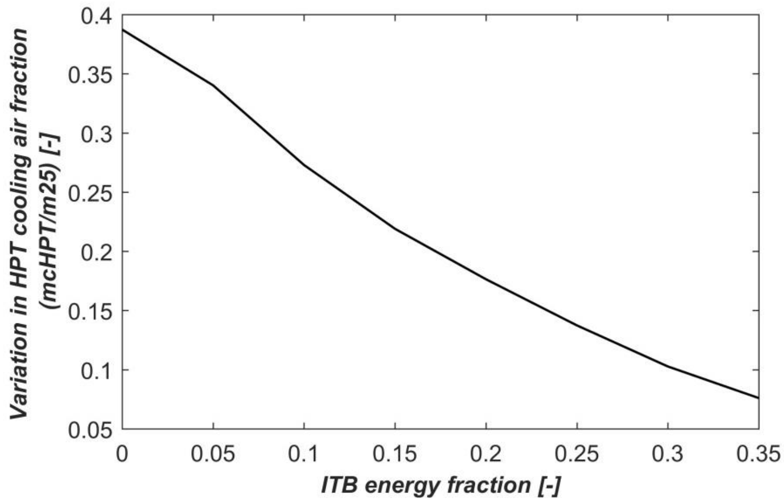


**Figure 13: Variation of the high pressure turbine (HPT) cooling requirement versus ITB energy fraction.**

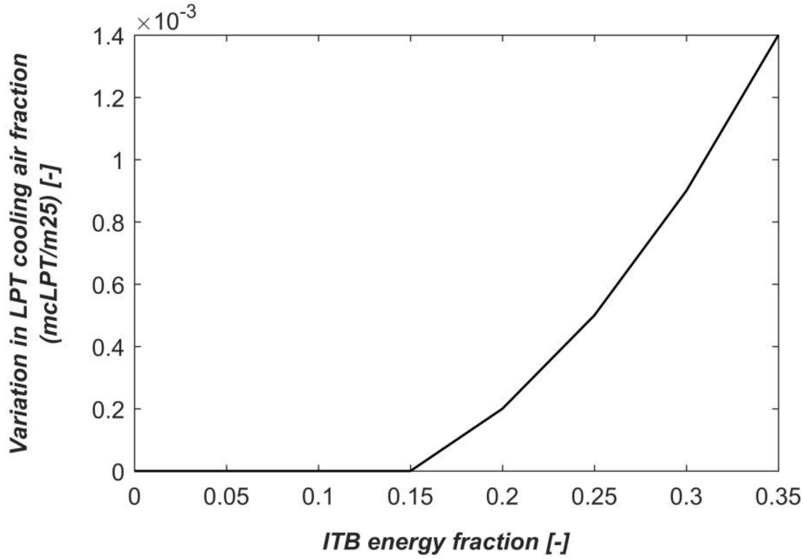


**Figure 14: Variation in low pressure turbine (LPT) cooling requirement versus ITB energy fraction.**

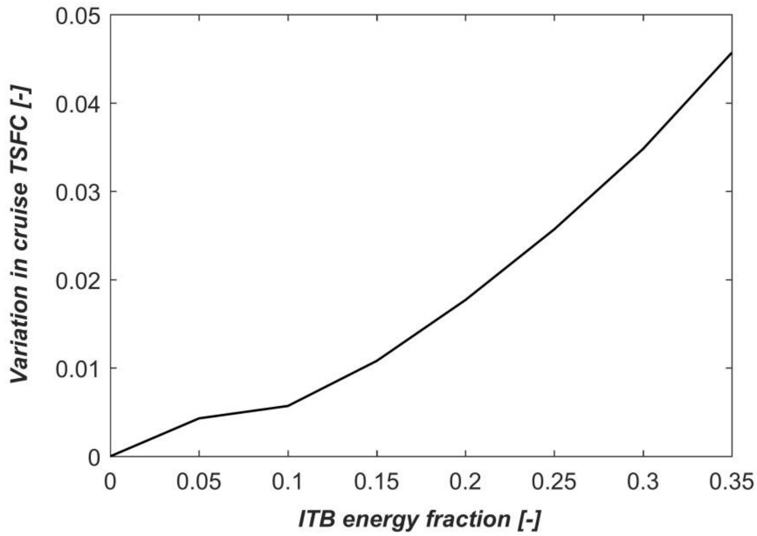


**Figure 15: Variation in cruise Thrust Specific Fuel Consumption(TSFC) versus ITB energy fraction.**

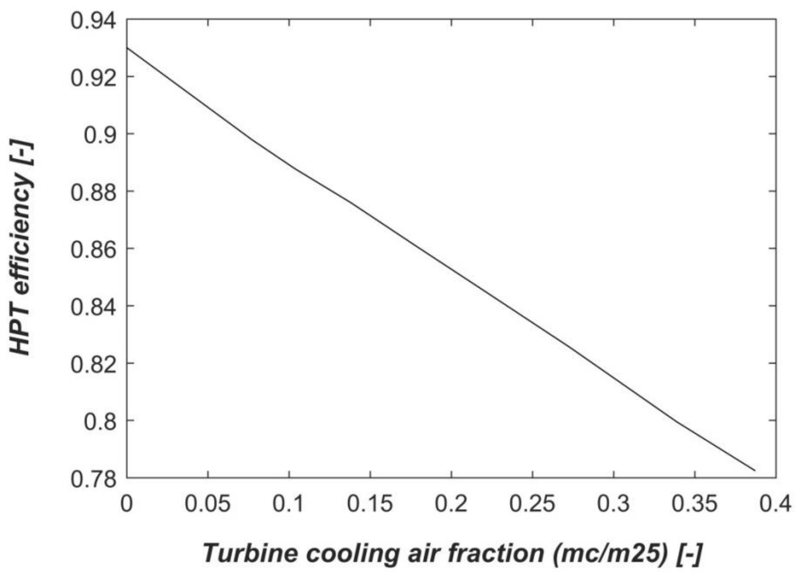


**Figure 16: Variation of the HPT polytropic efficiency versus the cooling fraction.**

Figure 17 shows the variation of engine thermal efficiency and propulsive efficiency for various ITB energy fractions at cruise condition. Since the specific thrust for each engine cycle is kept the same, the propulsive efficiency remains nearly constant for all engine types. However, the thermal efficiency reduces with increasing energy fraction because the combustion in ITB takes place at a lower pressure (when compared to the main combustion chamber).

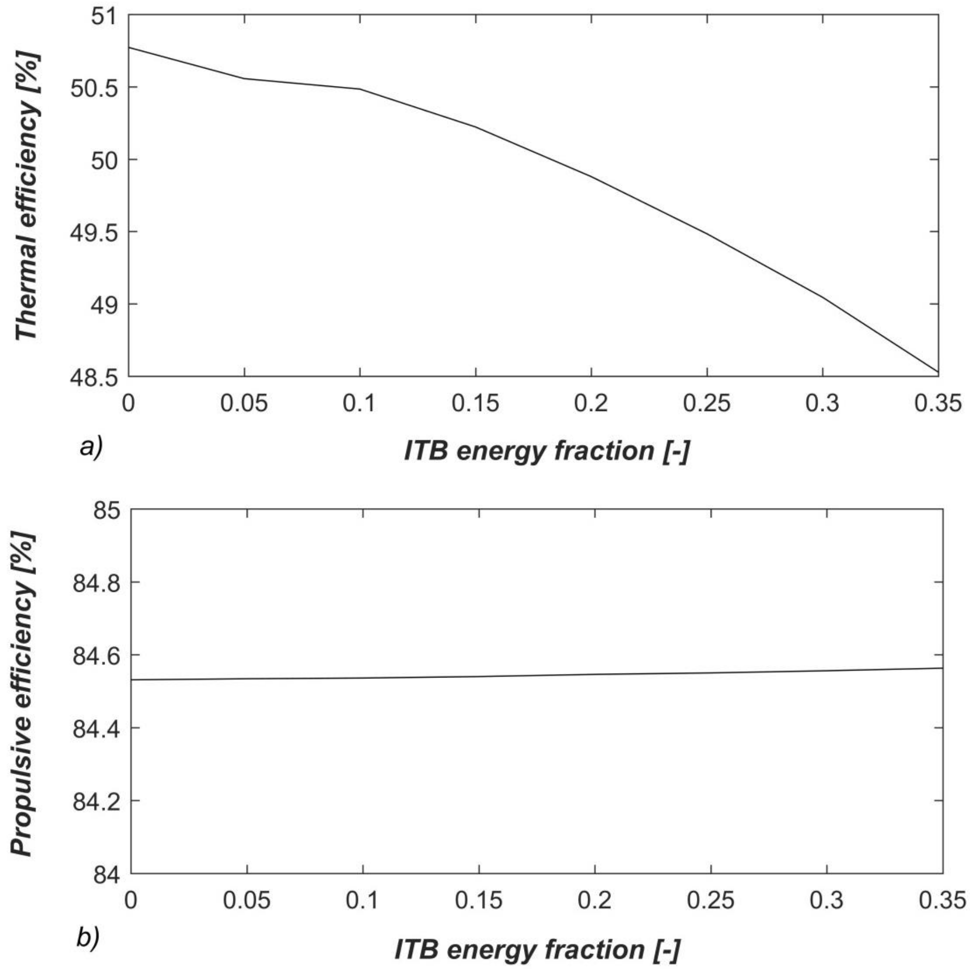


**Figure 17: a) Variation in the thermal efficiency at cruise; b) Variation in the propulsive efficiency at cruise.**

### C. Effects of ITB on NOx emission

The effects of the ITB on NOx emission is studied at SLS hot day take-off condition. The engine operating data is obtained from simulations executed in the previous section. The reactor setup presented in Figure 11 is used to evaluate NOx emission for each operating condition. To calculate the total NOx emission for GITB engine, the emission from each of the combustor must be evaluated. The combustor inlet conditions, gas composition and operating parameters are required. The values of these combustor operating parameters for various energy fractions is given in Table 6. Moreover, the calculated overall EINOx at different ITB energy fractions is presented in Table 6.

**Table 6: Inputs for the NOx emissions prediction at SLS ISA+15K**

| ***Input parameters*** | ***ITB energy fraction*** | | | | |
|---|---|---|---|---|---|
| | 0 | 0.1 | 0.2 | 0.3 | 0.35 |
| $T_{t3}$, K | 1049 | 1049 | 1049 | 1049 | 1049 |
| $p_{t3}$, Bar | 66.65 | 66.60 | 66.55 | 66.51 | 66.50 |
| $\dot{m}_3$, kg/s | 46.83 | 55.58 | 62.93 | 68.49 | 70.48 |
| $\dot{m}_{f_1}$, kg/s | 1.98 | 1.8 | 1.62 | 1.45 | 1.36 |
| $T_{t45}$, K | 1422 | 1353 | 1284 | 1214 | 1179 |
| $p_{t45}$, Bar | 16.14 | 15.76 | 15.22 | 14.52 | 14.10 |
| $\dot{m}_{45}$, kg/s | 78.44 | 78.24 | 78.03 | 77.79 | 77.65 |
| $\dot{m}_{f_2}$, kg/s | 0 | 0.2 | 0.41 | 0.62 | 0.73 |
| ***Output parameters*** | | | | | |
| Total EINOx, g/kg | 125.3 | 91.3 | 83.9 | 77.4 | 74.2 |

Figure 18 presents the variation in total NOx Emission Index (EINOx) versus the ITB energy fraction. The baseline engine is an advanced GTF engine with an ITB energy fraction of zero. It can be observed that due to the reduced energy input in each of the combustor, the NOx emission is lower than the single combustor configuration. Moreover, due to the NOx re-burning process in the ITB, a fraction of the NOx formed in the first combustor dissociates in the ITB, thereby reducing the total NOx emission at the exit of the ITB. Overall, the NOx emission reduce as the ITB energy fraction increases. It can be seen that the NOx emission can be reduced by up to 40% for an ITB energy fraction of 0.35. However, the penalty incurred in the thermal efficiency due to higher ITB energy fraction should be taken into account, as discussed in the previous section. It should be noted that the above analysis and estimates about NOx reduction are conservative as the ITB is assumed to be similar as the main combustor in the current analysis. The ITB could be incorporated within the inter turbine duct and novel combustion techniques like flameless combustion could be used to reduce the NOx emission even further, as elaborated by Rao & Bhat [34].

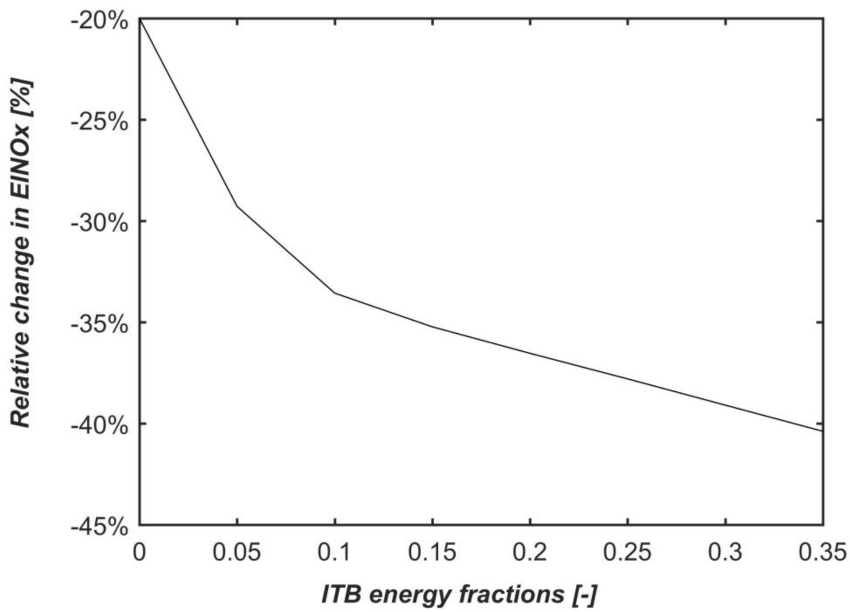


**Figure 18: Variation in NOx emission with ITB energy fraction at SLS ISA+15 K**

## VI. Conclusions

This analysis performed in this paper enables us to understand the potential advantages of using an Interstage Turbine Burner in a commercial VHBR turbofan engine. Primarily, the effect of the ITB on turbine cooling, NOx emission and fuel consumption has been presented. Several conclusions can be drawn from this research.

- The implementation of ITB helps to reduce the HPT operating temperature substantially, thereby resulting in a reduction in HPT cooling air requirement substantially, by up to 80%. This reduction in cooling air flow has a positive influence on HPT efficiency and the HPT operating life.
- The LPT cooling requirement is negligible (less than 0.2%) up to an ITB energy fraction of 0.35.
- The implementation of ITB reduces the thermal efficiency of the engine due to the pressure losses and heat addition at lower pressure; however, the improvement in turbine efficiency due to reduction in cooling can mitigate this effect to a large extent.
- With reduced energy input in each combustor and "NOx re-burning" in the ITB, the proposed GITB turbofan can reduce the NOx emission by up to 40% when compared to a contemporary GTF engine. This reduction is conservative, novel combustion techniques such as flameless combustion (as elaborated by Rao & Bhat) could be employed in ITB to reduce the NOx emission even further.

- Just as the addition of the gear on the LP spool helped to increase the engine propulsive efficiency without compromising the thermal efficiency, the ITB could help the engine to increase the engine OPR and TIT without compromising the engine NOx emission.

## References


1. ICAO Environmental report 2010, *Aircraft Technology Improvements*, 2010.

2. Lee, D. S., Fahey, D. W., Forster, P. M., Newton, P. J., Wit, R. C. N., Lim, L. L., Owen, B., and Sausen, R., *Aviation and global climate change in the 21st century,* Atmospheric Environment, 2009. 43.

3. Joyce E. Penner, David H. Lister, David J. Griggs, David J. Dokken, and Mack Macfraland, *Aviation and the global atmosphere*, Intergovernmental Panel on Climate Change, Cambridge University Press, Cambridge, UK, 1999.

4. Advisory Council for Aeronautics Research in Europe (ACARE), *Flightpath 2050 Europe's vision for aviation,* Luxembourg: Publications Office of the European Union, 2011.

5. Saravanamuttoo, H. I. H., Rogers, G. F. C., and Cohen, H., *Gas turbine theory*. 6th ed. 2008: Longman imprint.

6. Horlock, J., Watson, D., and Jones, T., *Limitations on gas turbine performance imposed by large turbine cooling flows,* Journal of engineering for gas turbines and power, 2001. 123(3): p. 487-494.

7. Wilcock, R., Young, J., and Horlock, J., *The effect of turbine blade cooling on the cycle efficiency of gas turbine power cycles,* Journal of Engineering for Gas Turbines and Power, 2005. 127(1): p. 109-120.

8. Lefebvre, A. H. and Ballal, D. R., *Gas Turbine Combustion: Alternative Fuels and Emissions, Third Edition*. 2010. Boca Raton, F.L.: CRC Press Taylor & Francis Group.

9. *https://easa.europa.eu/document-library/icao-aircraft-engine-emissions-databank*, [cited 2015 August].

10. Riegler, C. and Bichlmaier, C., *The Geared Turbofan Technology–Opportunities, Challenges and Readiness Status*. 1st CEAS European air and space conference, Berlin, Germany, 2007. p. 10-13.

11. Kyprianidis, K. G., Grönstedt, T., Ogaji, S. O. T., Pilidis, P., and Singh, R., *Assessment of Future Aero-engine Designs With Intercooled and Intercooled Recuperated Cores,* Journal of Engineering for Gas Turbines and Power, 2011. 133(1): p. 011701, DOI: 10.1115/1.4001982.

12. Petit, O., Xisto, C., Zhao, X., and Grönstedt, T., *An Outlook for Radical Aero Engine Intercooler Concepts*. in *ASME Turbo Expo 2016: Turbomachinery Technical Conference and Exposition*. 2016. American Society of Mechanical Engineers. p. V003T06A019-V003T06A019.

13. Kyprianidis, K. G. and Rolt, A. M., *On the Optimization of a Geared Fan Intercooled Core Engine Design*, Journal of Engineering for Gas Turbines and Power, 2015. 137(4): p. 041201.

14. Sirignano, W. and Liu, F., *Performance increases for gas-turbine engines through combustion inside the turbine,* Journal of Propulsion and Power, 1999. 15(1): p. 111-118.

15. Liu, F. and Sirignano, W. A., *Turbojet and turbofan engine performance increases through turbine burners*, Journal of Propulsion and Power, 2001. 17(3): p. 695-705, DOI: 10.2514/2.5797.

16. Chen, G., Hoffman, M. A., and Davis, R. L., *Gas-turbine performance improvements through the use of multiple turbine interstage burners*, Journal of propulsion and power, 2004. 20(5): p. 828-834.

17. Liew, K. H., *Aerothermodynamic cycle analysis of a dual-spool, separate-exhaust turbofan engine with an interstage turbine burner*, 2006. Michigan Technological University.

18. Güthe, F., Hellat, J., and Flohr, P., *The reheat concept: the proven pathway to ultralow emissions and high efficiency and flexibility,* J. Eng Gas Turb Power, 2009. 131(2): p. 1-7, DOI: 10.1115/1.2836613.

19. Lee, A. S., Singh, R., and Probert, S., *Two-combustor Engines' Performances under Design and Off*-design *Conditions*. in *45th AJAA/ASME/SAE/ASEE Joint Propulsion Conference & Exhibit*. 2009.

20. Grönstedt, T. and Avellán, R., *Mission Analysis of an Inter-Turbine Burning Turbofan Engine*. XXth International Symposium on Air Breathing Engines 2011 (ISABE 2011), Gothenburg, Sweden, 2011. p. 11.

21. Liew, K., Urip, E., and Yang, S., *Parametric cycle analysis of a turbofan engine with an interstage turbine burner*, Journal of propulsion and power, 2005. 21(3): p. 546-551, DOI: 10.2514/1.2546.

22. Walsh, P. P. and Flectcher, P., *Gas Turbine Performance*. 2nd ed. 2004. Oxford, UK: Blackwell Science

23. Visser, W. P. and Broomhead, M. J., *GSP, a generic object-oriented gas turbine simulation environment*. in *ASME Turbo Expo 2000: Power for Land, Sea, and Air*. 2000. American Society of Mechanical Engineers. p. V001T01A002-V001T01A002.

24. Han, J. C., Dutta, S., and Ekkad, S., *Gas turbine heat transfer and cooling technology*. 2012: CRC Press.

25. Halila, E., Lenahan, D., and Thomas, T., *Energy efficient engine high pressure turbine test hardware detailed design report,* 1982.

26. Stearns, E. M., *Energy efficient engine core design and performance report*, 1982.

27. Tiemstra, F. S., *Design of a Semi-Empirical Tool for the Evaluation of Turbine Cooling Requirements in a Preliminary Design Stage*, 2014. Master thesis. Delft University of Technology.

28. Hartsel, J., *Prediction of effects of mass-transfer cooling on the blade-row efficiency of turbine airfoils*, in *10th Aerospace Sciences Meeting*. 1972. American Institute of Aeronautics and Astronautics.

29. Kurzke, J., *Performance modeling methodology: efficiency definitions for cooled single and multistage turbines*. in *ASME Turbo Expo 2002: Power for Land, Sea, and Air*. 2002. American Society of Mechanical Engineers. p. 85-92.

30. Young, J. and Horlock, J., *Defining the efficiency of a cooled turbine*, Journal of turbomachinery, 2006. 128(4): p. 658-667.

31. Horlock, J. and Torbidoni, L., *Calculations of cooled turbine efficiency*, Journal of Engineering for Gas Turbines and Power, 2008. 130(1): p. 011703.

32. Lefebvre, A. H., *Fuel effects on gas turbine combustion-liner temperature, pattern factor, and pollutant emissions*, Journal of Aircraft, 1984. 21(11): p. 887-898.

33. Rizk, N. K. and Mongia, H., *Semianalytical correlations for NOx, CO, and UHC emissions*, Journal of Engineering for Gas Turbines and Power, 1993. 115(3): p. 612-619.

34. Rao, A. G. and Bhat, A., *Hybrid Combustion System for Future Aero Engines*. in *Proceedings of the 2nd National Propulsion Conference*. 2015. IIT Bombay, Powai, Mumbai. p. 1-9.

35. *http://www.cantera.org/docs/sphinx/html/reactors.html*, [cited 2015 August].

36. Shakariyants, S. A., *Generic methods for aero-engine exhaust emission prediction*, 2008. Doctoral Thesis. TU Delft, Delft University of Technology.

37. Dagaut, P., *On the kinetics of hydrocarbons oxidation from natural gas to kerosene and diesel fuel*, Physical Chemistry Chemical Physics, 2002. 4(11): p. 2079-2094, DOI: 10.1039/B110787A.

38. Honnet, S., Seshadri, K., Niemann, U., and Peters, N., *A surrogate fuel for kerosene*, Proceedings of the Combustion Institute, 2009. 32(1): p. 485-492, DOI: http://dx.doi.org/10.1016/j.proci.2008.06.218.

39. Telidevara, S., *Emissions Prediction in RQL based Aero Engines*, 2015. MSc thesis. Delft University of Technology.

40. Kathleen M Tacina, Chi-Ming Lee, and Changlie Wey, *NASA Glenn high pressure low NOx emissions research*, 2008.

41. Tacina, R., Mao, C. P., and Wey, C., *Experimental investigation of a multiplex fuel injector module for low emission combustors*. in *41st Aerospace Sciences Meeting and Exhibit*. 2003. p. 827.

42. *http://nl.mathworks.com/help/optim/ug/fmincon.html*, [cited 2015 August].

43. Nocedal, J. and Wright, S., *Numerical optimization*. 2nd ed. 2006: Springer Science & Business Media.

44. Lakshminarayana, B., *Methods of predicting the tip clearance effects in axial flow turbomachinery*, Journal of Fluids Engineering, 1970. 92(3): p. 467-480.